

Estimation of Concept Explanations Should be Uncertainty-Aware

Vihari Piratla
University of Cambridge
vp421@cam.ac.uk

Juyeon Heo*, Katherine Collins*, Sukriti Singh*
University of Cambridge

Adrian Weller
University of Cambridge
Alan Turing Institute

Abstract

Model explanations can be valuable for interpreting and debugging predictive models. We study a specific kind called Concept Explanations, where the goal is to interpret a model using human-understandable concepts. Although popular for their easy interpretation, concept explanations are known to be noisy. We begin our work by identifying various sources of uncertainty in the estimation pipeline that lead to such noise. We then propose an uncertainty-aware Bayesian estimation method to address these issues, which readily improved the quality of explanations. We demonstrate with theoretical analysis and empirical evaluation that explanations computed by our method are robust to train-time choices while also being label-efficient. Further, our method proved capable of recovering relevant concepts amongst a bank of thousands, in an evaluation with real-datasets and off-the-shelf models, demonstrating its scalability. We believe the improved quality of uncertainty-aware concept explanations make them a strong candidate for more reliable model interpretation. We release our code at <https://github.com/vps-anonconfs/uace>.

1 Introduction

As increasingly complex machine learning (ML) systems proliferate into real-world decision-making and reasoning, there is a growing need to be able to explain such systems. Concept-based explanations are a class of interpretable methods that explain predictions using high-level and semantically meaningful concepts [Kim et al., 2018]. Concept explanations are aligned with how humans communicate their decisions [Yeh et al., 2022] and are shown [Kim et al., 2018, 2023b] to be more preferable over explanations using salient input features [Ribeiro et al., 2016, Selvaraju et al., 2017] or salient training examples [Koh and Liang, 2017]. Concept explanations also show promise for encoding task-specific prior knowledge [Yuksekgonul et al., 2022] and propelling scientific discovery [Yeh et al., 2022].

Concept explanations offer insight into a pretrained prediction model by estimating the importance of concepts using two human-provided resources: (1) a list of potentially relevant concepts for the task, and (2) a dataset of examples, often referred to as the “probe-dataset”. Estimation typically proceeds in two steps: (a) compute the log-likelihood of a concept given an example called concept activations, and (b) aggregate their per-example activation scores into a globally relevant explanation. For example, the concept *wing* is considered important if the information about the concept

*equal contribution

is encoded in all examples of the *plane* class in the dataset. Owing to their model-level granularity, concept explanations are easy to interpret and have witnessed wide recognition in diverse applications [Yeh et al., 2022].

Notwithstanding their popularity, concept explanations are known to be noisy and data expensive. Ramaswamy et al. [2022a] showed that existing estimation methods are sensitive to the choice of concept set and dataset raising concerns over their interpretability. Another major limitation of concept-based explanation is the need for datasets with explicit concept annotations. Increasingly popular multimodal models such as CLIP [Radford et al., 2021] present an exciting alternate direction to specify relevant concepts, especially for common image applications, through their text description. Recent work has explored using multimodal models for training Concept Bottleneck Models (CBMs) [Oikarinen et al., 2023, Yuksekgonul et al., 2022, Moayeri et al., 2023], but they are not yet evaluated for generating post-hoc concept explanations.

Our objective is to improve the quality of concept explanations while also not requiring datasets with concept annotations. We begin by observing that existing estimation methods do not model uncertainty in the estimation pipeline, leading to high variance or noisy explanations. We identify at least *two sources of uncertainty* in the standard estimation of concept explanations. First, *when a concept is missing from the probe-dataset*, we cannot estimate its importance with confidence. Reporting uncertainty over estimated importance of a concept can thus help the user draw a more informed interpretation. Second, *when a concept is hard to recognize, or irrelevant to the task*, the corresponding activations predicted from the representation layer of the model-to-be-explained are expected to be noisy. If not modelled, uncertainty over concept activations either due to their absence, hardness, or relevance cascades into noise in explanations. Appreciating the need to model uncertainty, we present an estimator called **Uncertainty-Aware Concept Explanations (U-ACE)**, which we show is instrumental in improving quality of explanations.

Contributions. • We motivate the need for modelling uncertainty for faithful estimation of concept explanations. • We propose a **Bayesian estimation method** called U-ACE that is both **label-free** and **models uncertainty in the estimation of concept explanations**. • We demonstrate the merits of our proposed method U-ACE through theoretical analysis and empirical evidence on two controlled and three real-world datasets.

2 Background and Motivation

We denote the model-to-be explained as $f : \mathbb{R}^D \rightarrow \mathbb{R}^L$ that maps D-dimensional inputs to L labels. Let $f^{[l]}(\mathbf{x})$ denote the l^{th} layer representation space and $f(\mathbf{x})[y]$ for $y \in [1, L]$ be the logit for the label y . Given a probe-dataset of examples $\mathcal{D} = \{\mathbf{x}^{(i)}\}_{i=1}^N$ and a list of concepts $\mathcal{C} = \{c_1, c_2, \dots, c_K\}$, our objective is to explain the pretrained model f using the specified concepts. Traditionally, the concepts are demonstrated using potentially small and independent datasets with concept annotations $\{\mathcal{D}_c^k : k \in [1, K]\}$ where \mathcal{D}_c^k is a dataset with positive and negative examples of the k^{th} concept.

Concept-Based Explanations (CBE) proceed in two steps. In the first step, they learn **concept activation vectors (CAVs)** that predict the concept from l^{th} layer representation of an example. More formally, they learn the concept activation vector v_k for k^{th} concept by optimizing $v_k = \arg \min_v \mathbb{E}_{(x,y) \sim \mathcal{D}_c^k} [\ell(v^T f^{[l]}(\mathbf{x}), y)]$ where ℓ is the usual cross-entropy loss. The inner product of the representation with the concept activation vector $v_k^T f^{[l]}(\mathbf{x})$ is usually referred to as the **concept activations**. Various approaches exist to aggregate example-specific concept activations into model-level explanations for the second step. Kim et al. [2018] computes sensitivity of logits to interventions on concept activations to compute what is known as the CAV score per example per concept and report the fraction of examples in the probe-dataset with a positive CAV score as the global importance of the concept known as TCAV score. Zhou et al. [2018] proposed to decompose the classification layer weights as $\sum_k \alpha_k v_k$ and report the coefficients α_k as the importance score of the k^{th} concept. We refer the reader to Yeh et al. [2022] for an in-depth survey.

Data-efficient concept explanations. A major limitation of traditional CBEs is their need for datasets with concept annotations $\{\mathcal{D}_c^1, \mathcal{D}_c^2, \dots\}$. In practical applications, we may wish to find important concepts among thousands of potentially relevant concepts, which is not possible with-

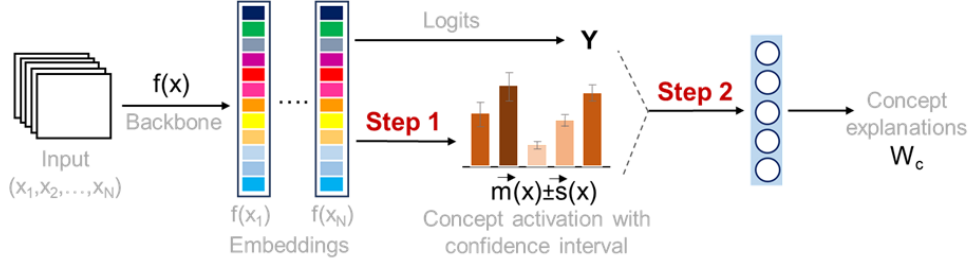


Figure 1: Our proposed estimator: Uncertainty-Aware Concept Explanations (U-ACE). We track uncertainty in concept activation scores from Step 1, and model them in Step 2.

out expensive data collection. Recent proposals [Yuksekgonul et al., 2022, Oikarinen et al., 2023, Moayeri et al., 2023] suggested using pretrained multimodal models like CLIP to evade the data annotation cost for a related problem called Concept Bottleneck Models (CBM) [Koh et al., 2020]. CBMs aim to train inherently interpretable model with a concept bottleneck. Although CBMs cannot generate explanations for a model-to-be-explained, a subset of methods propose to train what are known as Posthoc-CBMs using the representation layer of a pretrained task model for data efficiency. Given that Posthoc-CBMs base on the representation of a pretrained task model, we may use them to generate concept explanations. We describe briefly two such CBM proposals below.

Oikarinen et al. [2023] (O-CBM) estimates the concept activation vectors by learning to linearly project from the representation space of CLIP where the concept is encoded using its text description to the representation space of the model-to-be-explained f . It then learns a linear classification model on concept activations and returns the weight matrix as the concept explanation. Based on the proposal of Yuksekgonul et al. [2022], we can also generate explanations by training a linear model to match the predictions of model-to-be-explained directly using the concept activations of CLIP, which we denote by (Y-CBM).

Noisy explanations. Alongside data inefficiency, concept explanation methods are known to be noisy. We observed critical concerns with existing CBEs in the same spirit as the challenges raised in Ramaswamy et al. [2022a]. As we demonstrate in Sections 5, 6.1, G.1, concept explanations for the same model-to-be-explained vary with the choice of the probe-dataset or the concept set bringing into question the reliability of explanations.

3 Uncertainty-Aware Concept Explanations

As summarized in the previous section, CBEs rely on concept activations for generating explanations. It is not hard to see that the activation score of a concept cannot be predicted confidently if the concept is hard/ambiguous, or if it is not encoded by the model-to-be-explained. Moreover, the importance of a concept cannot be confidently estimated if it is missing from the probe-dataset. Motivated by the need to model uncertainty in the estimation, we design our estimator: U-ACE.

Our approach encompasses the following steps: (1) estimate concept activations along with their error interval, and (2) aggregate concept activations and their confidence intervals in to a global concept explanation. We describe the estimation of concept activations and their error given an instance x denoted as $\vec{m}(x), \vec{s}(x)$ respectively in Section 3.1. By definition, the true concept activation for a concept k and instance x is in the range of $\vec{m}(x) \pm \vec{s}(x)$ with a high probability. We describe the estimation of concept explanations in what follows using $\vec{m}(x), \vec{s}(x)$, which is independent of how they are computed.

We compute explanations by fitting a linear regression model on the concept activations in the same spirit as many CBM methods as it is easier to incorporate the input noise in a regression model. Our objective is to learn linear model weights W_c of size $L \times K$ (recall that L, K are the number of labels and concepts respectively) that map the concept activations to their logit scores, i.e. $f(x) \approx W_c \vec{m}(x)$. Since the concept activations contain noise, we require that W_c is such that predictions do not change under noise, that is $W_c[\vec{m}(x) + \vec{s}(x)] \approx W_c \vec{m}(x) \implies W_c \vec{s}(x) \approx 0$. I.e. the inner product of each row (\vec{w}) of W_c with $\vec{s}(x)$ must be negligible. For the sake of exposition, we analyse

the solution of $\mathbf{y}^{th} \in [1, L]$ row \vec{w} of W_c , which can be easily generalized to the other rows. We cast the bounded error constraint, i.e. $|\vec{w}^T \vec{s}(\mathbf{x})| \leq \delta$ for some small positive δ and for all the instances \mathbf{x} in the probe-dataset, into a distributional prior over the weights as shown below.

The per-example constraint $|\vec{w}^T \vec{s}(\mathbf{x})| \leq \delta$ leads to the following constraint with the average noise.

$$|\vec{w}^T \epsilon| \leq \frac{\sum_{\mathbf{x} \in \mathcal{D}} |\vec{w}^T \vec{s}(\mathbf{x})|}{N} \leq \delta \text{ where } \epsilon \triangleq \frac{\sum_{\mathbf{x} \in \mathcal{D}} \vec{s}(\mathbf{x})}{N}$$

If we require that the dot-product with the average noise be bounded, i.e. $|\vec{w}^T \epsilon| \leq \delta$, for some small $\delta > 0$ with high probability, their norm, $\vec{w}^T \epsilon \epsilon^T \vec{w}$, must be bounded. If we then approximate $\epsilon \epsilon^T$ with the positive semi-definite $\text{diag}(\epsilon \epsilon^T)$, we can pose the constraint as a distributional prior as below.

$$\begin{aligned} \vec{w}^T \text{diag}(\epsilon \epsilon^T) \vec{w} &\leq \delta^2 \\ \Rightarrow -\frac{1}{2}(\vec{w} - \mathbf{0})^T S^{-1}(\vec{w} - \mathbf{0}) &\text{ where } S^{-1} = \text{diag}(\epsilon \epsilon^T) \\ \text{is high when } \vec{w} &\text{ satisfies the constraint} \\ \Rightarrow \mathcal{N}(\vec{w}; \mathbf{0}, \lambda S) &\text{ is high for an appropriate } \lambda > 0 \\ \Rightarrow \vec{w} \sim \mathcal{N}(\mathbf{0}, \lambda S) \end{aligned}$$

We observe therefore that the weight vectors drawn from $\mathcal{N}(\mathbf{0}, \lambda \text{diag}(\epsilon \epsilon^T)^{-1})$ satisfy the invariance to input noise constraint with high probability. We now estimate the posterior on the weights after having observed the data with the prior on weights set to $\mathcal{N}(\mathbf{0}, \lambda \text{diag}(\epsilon \epsilon^T)^{-1})$. The posterior over weights has the following closed form [Salakhutdinov, 2011] where $C_X = [\vec{m}(\mathbf{x}_1), \vec{m}(\mathbf{x}_2), \dots, \vec{m}(\mathbf{x}_N)]$ is a $K \times N$ matrix and $Y = [f(\mathbf{x}_1)[y], f(\mathbf{x}_2)[y], \dots, f(\mathbf{x}_N)[y]]^T$ is an $N \times 1$ vector (derivation in Appendix A.1).

$$\begin{aligned} \Pr(\vec{w} \mid C_X, Y) &= \mathcal{N}(\vec{w}; \mu, \Sigma) \\ \text{where } \mu &= \beta \Sigma C_X Y, \quad \Sigma^{-1} = \beta C_X C_X^T + \lambda^{-1} \text{diag}(\epsilon \epsilon^T) \end{aligned} \quad (1)$$

β is the inverse variance of noise in observations Y . We optimise both β and λ using MLE on \mathcal{D} (more details in Appendix B). We could directly set the inverse of β approximately 0 since there is no noise on the observations Y . Instead of setting β to an arbitrary large value, we observed better explanations when we allowed the tuning algorithm to find a value of β, λ to balance the evidence and noise.

The estimator shown in Equation 1 is how we model noise in U-ACE. In the next section, we describe how we may estimate the noise in the concept activations. Algorithm 1 summarizes our proposal.

3.1 Estimation of concept activations and their noise

In this section, we discuss how we estimate $\vec{m}(\mathbf{x}), \vec{s}(\mathbf{x})$ using a pretrained multimodal model. Recall that image-text multimodal (MM) systems such as CLIP [Radford et al., 2021] can embed both images and text in a shared representation space, which enables one to estimate the similarity of an image to any phrase. This presents us with the flexibility to specify a concept using its text description (T_k for the k^{th} concept) without needing concept datasets \mathcal{D}_c^k . We denote by $g(\bullet)$ the image embedding function of MM and $g_{text}(\bullet)$ the text embedding function.

Our objective is to estimate $\vec{m}(\mathbf{x}), \vec{s}(\mathbf{x})$ such that the true concept activation value is in the range $\vec{m}(\mathbf{x}) \pm \vec{s}(\mathbf{x})$. Two major sources of uncertainty in concept activations that must inform $s(\mathbf{x})$ are due to (1) *epistemic (model) uncertainty* arising from lack of information about the concept in the representation layer of the model-to-be-explained, (2) *data uncertainty* arising from ambiguity (because the concept is not clearly visible, see Figures 7, 8, 9, 10 of Appendix H.1 for some examples). We wish to estimate $\vec{s}(\mathbf{x})$ that is aware of both the forms of uncertainty.

We can obtain a point estimate for the activation vector of the k^{th} concept v_k such that $f(\mathbf{x})^T v_k \approx g(\mathbf{x})^T w_k$ (where $w_k = g_{text}(T_k)$) for all \mathbf{x} in the probe-dataset \mathcal{D} through simple optimization [Oikarinen et al., 2023, Moayeri et al., 2023]. We may then simply repeat the estimation procedure multiple times to sample from the distribution of activation vectors and their corresponding concept activations. However, as shown empirically in Appendix H.1, $\vec{s}(\mathbf{x})$ estimated from random sampling is a poor measure of uncertainty, which is unsurprising for high dimensional spaces.

We instead derive a closed form for $\vec{m}(\mathbf{x}), \vec{s}(\mathbf{x})$ based on the following intuition. The concept activations estimated using $\cos\text{-sim}(f(\mathbf{x}), v_k)$ must intuitively be in the ballpark of $\cos(\theta_k) = \cos\text{-sim}(g(\mathbf{x}), w_k)$ where $\cos\text{-sim}$ is the cosine similarity [Wikipedia, 2023a] (we switched from dot-products to $\cos\text{-sim}$ to avoid differences due to magnitude of the vectors). However, if the concept k is not encoded in $f(\mathbf{x})$ or if it is ambiguous, the concept activations are expected to deviate by an angle α_k , which is an error measure specific to the concept. Therefore, we expect the concept activations to be in the range of $\cos(\theta_k \pm \alpha_k)$. The concept specific value α_k must account for uncertainty due to lack of knowledge (for eg. irrelevant concept) and due to ambiguity (for eg. concept is not clearly visible). In what follows, we present a specific measure for α_k and the closed form solution for $\vec{m}(\mathbf{x}), \vec{s}(\mathbf{x})$.

Borrowing from Oikarinen et al. [2023], we define $\cos(\alpha_k)$ as $\max_v [\cos\text{-sim}(e(v, f, \mathcal{D}), e(w_k, g, \mathcal{D}))]$ where $e(w_k, g, \mathcal{D}) \triangleq [w_k^T g(\mathbf{x}_1), \dots, w_k^T g(\mathbf{x}_N)]^T$, and $e(v, f, \mathcal{D}) \triangleq [v^T f^{[-1]}(\mathbf{x}_1), \dots, v^T f^{[-1]}(\mathbf{x}_N)]^T$. We may just as well adopt any other measure for α_k .

Proposition 1. *For a concept k and α_k defined as above, we have*

$$\vec{m}(\mathbf{x})_k = \cos(\theta_k)\cos(\alpha_k), \quad \vec{s}(\mathbf{x})_k = \sin(\theta_k)\sin(\alpha_k)$$

where $\cos(\theta_k) = \cos\text{-sim}(g_{\text{text}}(T_k), g(\mathbf{x}))$ and $\vec{m}(\mathbf{x})_k, \vec{s}(\mathbf{x})_k$ denote the k^{th} element of the vector.

The proof can be found in Appendix C. The mean and scale values above have a clean interpretation. If the model-to-be-explained (f) uses the k^{th} concept for label prediction, the information about the concept is encoded in f and we get a good fit, i.e. $\cos(\alpha_k) \approx 1$, and a small error on concept activations. On the other hand, error bounds are large and concept activations are suppressed when the fit is poor, i.e. $\cos(\alpha_k) \approx 0$.

Although $s(\mathbf{x})$ given by Proposition 1 is simple, we found it to be surprisingly effective, which are presented in Appendix H.1. The appendix section contains the following details. (1) We introduced two other variants for measuring uncertainty: Monte Carlo and a distribution fit method (based on [Kim et al., 2023a]). (2) We evaluated different methods for quantifying the different sources of uncertainty on a real dataset. Across different sources of uncertainty and uncertainty estimation methods, we found our method to be consistently effective.

3.2 Theoretical motivation

We now demonstrate theoretically the pitfalls of using a standard method for estimating concept explanations. For ease of analysis, we focus on robustness to misspecified concept sets. In our study, we compared explanations generated using a standard linear estimator (using Ordinary Least Squares [Wikipedia, 2024]) and U-ACE. Recall that Posthoc-CBMs (O-CBM, Y-CBM), which are our primary focus for comparison, both estimate explanations by fitting a linear model on concept activations.

We present two scenarios with noisy concept activations. In the first scenario (over-complete concept set), we analysed the estimation when the concept set contains many irrelevant concepts. We show that the likelihood of marking an irrelevant concept as more important than a relevant concept increases rapidly with the number of concepts when the explanations are estimated using a standard linear estimator, which is presented in Corollary 1. In the same result, we also demonstrated that U-ACE do not suffer the same problem. In the second scenario (under-complete concept set), we analysed the explanations when the concept set only includes irrelevant concepts, wherein both concepts should be assigned importance at or near zero. We again show in Proposition 3 that a standard linear model attributes a significantly non-zero score while U-ACE mitigates the issue.

Setting 1: Unreliable explanations due to over-complete concept set. We analyse a simple setting where the output (y) is linearly predicted from the input (\mathbf{x}) as $y = \mathbf{w}^T \mathbf{x}$. We wish to estimate the importance of some K concepts by fitting a linear estimator on concept activations. Where concept activations are computed as $\mathbf{w}_k^T \mathbf{x}$ using concept activation vectors (\mathbf{w}_k) that are distributed as $\mathbf{w}_k \sim \mathcal{N}(\mathbf{u}_k, \sigma_k^2 I), k \in [1, K]$.

Proposition 2. *The concept importance estimated by U-ACE when the input dimension is sufficiently large and for a regularizing hyperparameter $\lambda > 0$ is approximately given by $v_k = \frac{\mathbf{u}_k^T \mathbf{w}}{\mathbf{u}_k^T \mathbf{u}_k + \lambda \sigma_k^2}$.*

On the other hand, the importance scores estimated using a standard estimator under the same conditions is distributed as $v_k \sim \mathcal{N}(\frac{\mathbf{u}_k^T \mathbf{w}}{\mathbf{u}_k^T \mathbf{u}_k}, \sigma_k^2 \frac{\|\mathbf{w}\|^2}{\|\mathbf{u}_k\|^2})$.

Proof of the result can be found in Appendix D. Based on the result, we can deduce the following for a specific case of \mathbf{u}_k s and σ_k s.

Corollary 1. *For the data setup of Proposition 2, the following results holds when $\mathbf{u}_1 = \mathbf{w}$, $\sigma_1 \approx 0$ and $\mathbf{u}_k^T \mathbf{w} = 0$, $\forall k \in [2, K]$. Then the probability that the standard estimator returns the first concept as the most salient decreases exponentially with the number of concepts. On the other hand, the importance score assigned by U-ACE is 1 for the only relevant first concept and 0 otherwise.*

Derivation of the result can be found in Appendix E. We observe from the result that the standard estimator will more likely flag an irrelevant concept as relevant, which is addressed when using U-ACE. Section 5 confirms our theoretical observation in practice.

Setting 2: Unreliable explanations due to under-complete concept sets. We now analyse explanations when the concept set only includes two irrelevant concepts. Like in the previous setting, the k^{th} concept activation $c_k^{(i)}$ is computed as $\mathbf{w}_k^T \mathbf{x}^{(i)}$. Consider two orthogonal unit vectors \mathbf{u}, \mathbf{v} . We define the concept activations for the two concepts $c_1^{(i)}, c_2^{(i)}$ for the i^{th} instance $\mathbf{x}^{(i)}$ and label $y^{(i)}$ as below.

$$\begin{aligned} y^{(i)} &= \mathbf{u}^T \mathbf{x}^{(i)}, \quad c_1^{(i)} = (\beta_1 \mathbf{u} + (1 - \beta_1) \mathbf{v})^T \mathbf{x}^{(i)} \\ c_2^{(i)} &= (\beta_2 \mathbf{u} + (1 - \beta_2) \mathbf{v})^T \mathbf{x}^{(i)} \\ \text{where } \beta_1 &\sim \mathcal{N}(b_1, \sigma^2), \beta_2 \sim \mathcal{N}(b_2, \sigma^2) \end{aligned}$$

If b_1, b_2, σ^2 are very small, then both concepts are expected to be unimportant for label prediction due to small overlap with \mathbf{u} . However, we can see with some effort (Appendix F) that the importance scores computed by a standard estimator are $\frac{1-\beta_2}{\beta_1-\beta_2}, \frac{1-\beta_1}{\beta_1-\beta_2}$, which are large because $\beta_1 \approx 0, \beta_2 \approx 0 \therefore \beta_1 - \beta_2 \approx 0$. We will now show that U-ACE estimates near-zero importance scores as expected.

Proposition 3. *The importance score estimated by U-ACE is approximately $\frac{b_1/2}{1+\lambda\sigma^2}, \frac{b_2/2}{1+\lambda\sigma^2}$, where $\lambda > 0$ is a regularizing hyperparameter.*

Proof can be found in Appendix F. It follows from the result that the importance scores computed by U-ACE are near-zero for sufficiently large value of λ .

4 Experiments

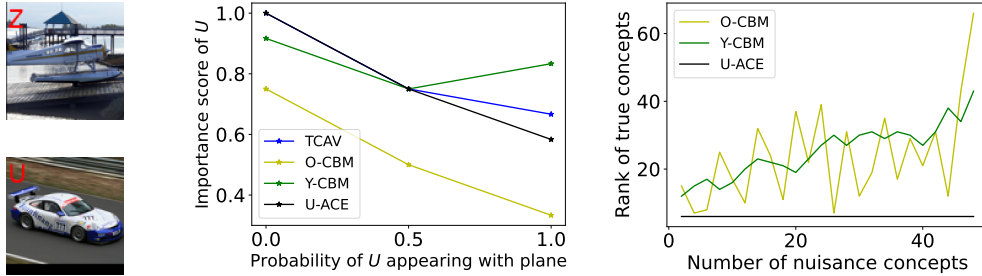


Figure 2: (Left) STL dataset with a spurious tag. (Middle) Importance of a tag concept for three different model-to-be-explained. X-axis shows the probability of tag in the training dataset of model-to-be-explained. (Right) Average rank of true concepts with irrelevant concepts; lower is better.

We now empirically evaluate U-ACE on synthetic and real datasets. We make a quantitative assessment with known ground-truth concepts on a controlled dataset in Section 5. In Section 6.1, we evaluate on two challenging real-world datasets with more than 700 concepts. Finally in Section 6.2, we evaluate utility of different methods in recovering known spurious features from more than 2,000 concepts.

Baselines. *Oracle*: Explanations are estimated using lasso regression of ground-truth concept annotations to estimate logit values of f . *Oracle* was also adopted in the past [Ramaswamy et al., 2022b,a]. Other baselines are introduced in Section 2: *TCAV* [Kim et al., 2018], *O-CBM* [Oikarinen et al., 2023], *Y-CBM* based on [Yuksekgonul et al., 2022].

Standardized comparison between importance scores. The interpretation of the importance score varies between different estimation methods. For instance, the importance score in *TCAV* is the fraction of examples that meet certain criteria, but for the rest the importance scores are the weights from linear model that predicts logits. Further, *Oracle* operates on binary concept annotations and *O-CBM*, *Y-CBM*, *U-ACE* on soft scores. For this reason, we cannot directly compare importance scores or their normalized variants. We instead use negative scores to obtain a ranked list of concepts and assign to each concept an importance score given by its rank in the list normalized by number of concepts. Our sorting algorithm ranks any two concepts with same score by alphabetical order of their text description. In all our comparisons we use the rank score if not mentioned otherwise.

Other experiment details. For all our experiments, we employed a Visual Transformer (with 32 patch size called “ViT-B/32”) based pretrained CLIP model that is publicly available for download at <https://github.com/openai/CLIP> as the pretrained multimodal model, which we denoted by g . We use $l = -1$, i.e. last layer just before computation of logits for all the explanation methods. *U-ACE* returns the mean and variance of the importance scores as shown in Algorithm 1, we use mean divided by standard deviation as the importance score estimated by *U-ACE* everywhere for comparison with other methods.

5 Assessment with known ground-truth

We now seek to establish that *U-ACE* generates faithful concept explanations. Subscribing to the common evaluation practice [Kim et al., 2018], we generate explanations for a model that is trained on a dataset with controlled correlation of a spurious pattern. We make a dataset using two labels from STL-10 dataset [Coates et al., 2011] *car*, *plane* and paste a tag U or Z in the top-left corner as shown in the left panel of Figure 2. The probability that the examples of *car* are added the Z tag is p and $1-p$ for the U tag. Conversely for the examples of *plane*, the probability of U is p and Z is $1-p$. We generate three training datasets with $p=0$, $p=0.5$ and $p=1$, and train three classification models using 2-layer convolutional network. As such, the three models are expected to have a varying and known correlation with the tag, which we hope to recover from its concept explanation.

We generate concept explanations for the three model-to-be-explained using a concept set that includes seven car-related concepts and three plane-related concepts (Appendix G) along with the two tags U , Z . We obtain the importance score of the concept U with *car* class using a probe-dataset that is held-out from the corresponding training dataset (i.e. probe-dataset has the same input distribution as the training dataset). The results are shown in the middle plot of Figure 2. Since the co-occurrence probability of U with *car* class goes from 1, 0.5 to 0 for $p=0, 0.5, 1$, we expect the importance score of U should change from positive to negative as we move right. We note that *U-ACE*, along with others, show the expected decreasing importance of the tag concept. The result corroborates that *U-ACE*, along with others, estimate a faithful explanation in the standard evaluation setting. Next, we evaluate robustness to misspecified or overly-complete concept set.

Unreliability due to a over-complete concept set. We generate explanations as animal (irrelevant and therefore nuisance) concepts are added (Appendix G contains the full list) to the relevant list of twelve original concepts. The right panel of Figure 2 depicts the average rank of true concepts (lower the better) with the number of irrelevant concepts on the horizontal axis. We note that *U-ACE* ranks true concepts highly even with 50 nuisance concepts while *O-CBM* and *Y-CBM* increasingly get worse with the number of irrelevant concepts as predicted by Corollary 1.

6 Real-world evaluation

We expect the improved modeling of our estimator to also generate higher-quality concept explanations in practice. To verify, we next explore explanations for two off-the-shelf pretrained models.

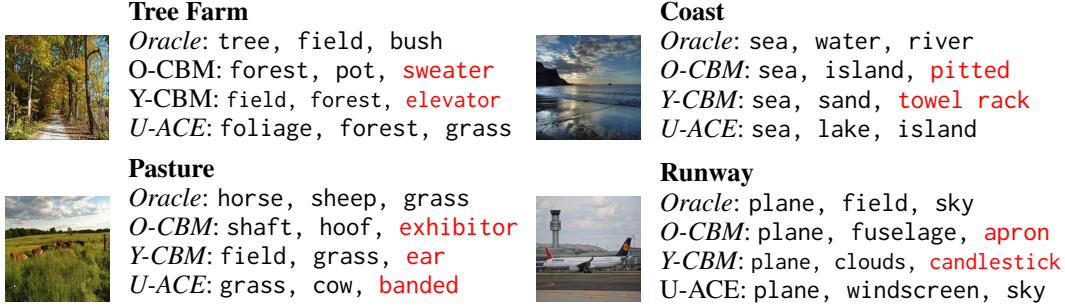


Figure 3: Two most relevant concepts plus any mistake (marked in red) from top-10 concepts for a scene-classification model estimated with various algorithms using PASCAL (left) or ADE20K (right) probe-dataset.

6.1 Scene Classification

In this section, we evaluate concept explanations obtained for a scene classification model with ResNet-18 architecture pretrained on the publicly available Places365 [Zhou et al., 2017a]. Following the experimental setting of Ramaswamy et al. [2022a], we generate explanations when the probe-dataset is set to PASCAL [Chen et al., 2014] or ADE20K [Zhou et al., 2017b], which are both part of the Broden dataset [Bau et al., 2017b]. The dataset contains images with dense annotations with more than 1000 attributes. Since it is irrational to explain a scene using scene concepts, we drop around 300 concepts that are marked as scene-related in the dataset. For the remaining 730 attributes, we defined a concept per attribute using literal name of the attribute. We picked 50 scene labels (Appendix G contains the full list) that have support of at least 20 examples in both ADE20K and PASCAL datasets.

We evaluate the quality of explanations by their closeness to the explanations generated using the *Oracle* baseline. Because *Oracle* fits an estimator using human-annotated concept labels, they are the closest to the ground-truth. For the top-20 concepts identified by *Oracle*, we compute the average absolute difference in importance scores estimated using any estimation method and *Oracle*. Table 1 presents the deviation in explanations averaged over all the 50 scene labels. Figure 3 shows the most salient concepts for four randomly picked scene labels. We observe from the figure that top-10 concepts identified by U-ACE seem more relevant to the scene when compared with Y-CBM and O-CBM. We also evaluated the explanation quality using a standard measure for comparing ranked lists, which is presented in Appendix G, which further confirms the dominance of U-ACE.

Dataset shift. Ramaswamy et al. [2022a] demonstrated with results the drastic shift in concept explanations for the same model-to-be-explained when using ADE20K or PASCAL as the probe-dataset. Explanations diverge partly because (a) population of concepts may vary between datasets thereby influencing their perceived importance when using standard methods, (b) noise in estimated explanations. We have demonstrated that U-ACE estimated importance scores have low noise and attributes high uncertainty and thereby near-zero importance to concepts that are rare or missing from the probe-dataset (Section G.1). For these reasons, we expect U-ACE to mitigate the data-shift problem. We confirm the same by estimating the average difference in importance scores estimated using ADE20K and PASCAL for different estimation techniques (where the average is only over salient concepts with non-zero importance). The results are shown in Table 2 and are inline with our prediction.

Dataset↓	TCAV	O-CBM	Y-CBM	U-ACE
ADE20K	0.13	0.19	0.16	0.09
PASCAL	0.41	0.20	0.18	0.11

Table 1: *Evaluation of explanation quality.* Each cell shows the average absolute difference of importance scores for top-20 concepts estimated using *Oracle*.

<i>Oracle</i>	TCAV	O-CBM	Y-CBM	U-ACE
0.41	0.41	0.32	0.33	0.19

Table 2: *Effect of data shift.* Average absolute difference between concept importance scores estimated using ADE20K and PASCAL datasets for the same model-to-be-explained using different estimation methods.

6.2 Object Classification

In this section, we evaluate explanations obtained for an object classification model with ResNet-18 architecture that was pretrained on the Imagenet dataset. Unlike for Broden dataset, Imagenet does not have annotations over concepts. As such, we evaluate the quality of explanations according to how effectively they bring out previously known incidental or spurious correlations of the dataset. Salient-Imagenet [Singla and Feizi, 2022] is an impressive annotation effort to identify prevalent and problematic dependence on co-occurring but irrelevant features for object recognition such as *door* feature when classifying *doormat*. We are interested in examining if we can discover such incidental features using concept explanations. We gathered 2,020 words by tokenising and filtering notes left by annotators of Salient-Imagenet, which we use as the concept set. One may also populate the concept set by generating a caption for each image using the pretrained multimodal model. For the sake of evaluation, we randomly identified 40 classes with at least one known incidental feature, and manually lexicalized the concept corresponding to the incidental feature for each class (see Appendix G.2 contains the full list).

In Table 3, we show the success of different estimation methods in discovering a known incidental correlation. We observe that U-ACE is the most effective in capturing the dependence. Although O-CBM and Y-CBM seem effective, we observed that they identified many nonsensical concepts (items that are very unlikely to be relevant) as relevant as shown in Table 4.

We are glad that U-ACE discovered known spurious features for 36 of the 40 labels (Table 3) with little effort while also being accurate (Table 4). However, our experiment only quantified recall of the spurious feature with only anecdotal evidence for precision. We leave for a future study a more tighter evaluation quantifying both recall and precision along with user studies to measure the utility of U-ACE for model debugging.

k	O-CBM	Y-CBM	U-ACE
10	14	22	25
25	23	28	33
50	31	29	36

Table 3: Number of classes (of the total 40) for which the known spurious feature is found in the top-k concepts estimated using different methods shown in the top-row.

howler monkey	Y-CBM	underside, monkey, cat
	O-CBM	polecat , porcupine , bear
	U-ACE	siamang, colobus, gibbon
coast	Y-CBM	shore, view , maillot
	O-CBM	beach, shore, tyre
	U-ACE	beach, sea, boats

Table 4: Top-2 concepts plus any mistake identified from top-10 important concepts shown in red. More results in Table 7

7 Related Work

Concept Bottleneck Models use a set of predefined human-interpretable concepts as an intermediate feature representation to make the predictions [Koh et al., 2020, Bau et al., 2017a, Kim et al., 2018, Zhou et al., 2018]. CBM allows human test-time intervention which has been shown to improve overall accuracy [Barker et al., 2023]. Traditionally, they require labelled data with concept

annotations and accuracy is typically worse than the standard models without concept bottleneck. To address the limitation of concept annotation, recent works have leveraged large pretrained multimodal models like CLIP [Oikarinen et al., 2023, Yuksekgonul et al., 2022]. Concept Embedding Models (CEM) [Espinosa Zarlenga et al., 2022] overcome the trade-off between accuracy and interpretability by learning high-dimensional concept embeddings. However, addressing the noise in the concept prediction remains underexplored. Collins et al. [2023] have studied *human* uncertainty in concept-based models and elucidate the importance of considering uncertainty over concepts in improving the reliability of the model. Closely related to our work, Kim et al. [2023a] propose the Probabilistic Concept Bottleneck Models (ProbCBM). They too argue for the need to model uncertainty in concept prediction for reliable explanations. However, their method of noise estimation in concept activations requires retraining the model and cannot be applied directly when concept activations are estimated using CLIP. Moreover, they use simple MC sampling to account for noise in concept activations, which is not nearly as effective (Appendix H.1).

Concept-based explanations use a separate probe dataset to first learn the concept and then explain through decomposition either the individual predictions or overall label features. Yeh et al. [2022] contains a brief summary of existing concept based explanation methods. Our proposed method is very similar to concept-based explanations (CBE) [Kim et al., 2018, Bau et al., 2017a, Zhou et al., 2018, Ghorbani et al., 2019]. Ramaswamy et al. [2022a] emphasised that the concepts learned are sensitive to the probe dataset used and therefore pose problems when transferring to applications that have distribution shift from the probe dataset. They further highlight the drawback of existing CBE methods that concepts can sometimes be harder to learn than the label itself (meaning the explanations may not be causal) and that the typical number of concepts used for explanations far exceed what a typical human can parse easily. Achibat et al. [2022] championed an explanation method that provides explanation highlighting important feature (answering “where”) and what concepts are used for prediction thereby combining the strengths of global and local explanation methods. Choi et al. [2023] have built upon the current developments in CBE methods for providing explanations for out-of-distribution detectors. Wu et al. [2023] introduced the causal concept based explanation method (Causal Proxy Model), that provides explanations for NLP models using counterfactual texts. Moayeri et al. [2023] also used CLIP to interpret the representations of a different model trained on uni-modal data.

8 Conclusion

We studied concept explanation methods with a focus on data-efficient systems that exploit pretrained multimodal models. We highlighted the quality challenge of the of existing estimators of concept explanations via simple examples and motivated the need for modelling *uncertainty* in their estimation. Accordingly, we proposed an uncertainty-aware and data-efficient estimator called U-ACE. We demonstrated the merits of our estimator through theoretical analysis, controlled study experiments and three challenging real-world evaluation with order of thousand concepts. Our results establish the strong promise of concept explanations estimated using our Bayesian method for effective model debugging.

Limitations and Future Work. Pretrained multimodal models enabled us to work with an open-world specification of the set of concepts, without necessitating expensive annotation data. Yet, dependence on a pretrained model may limit application in certain specialised domains, which while emerging in domains like healthcare [Huang et al., 2023], may temporarily hinder widespread adoption. In the same vein, an estimator that also models the uncertainty due to lack of knowledge of the pretrained multimodal model about a concept will be better suited for addressing any lapses in the pretrained model, which we leave for the future. Additionally, while we do not run user studies in this work, a natural and exciting next step is to explore whether U-ACE explanations are preferred by real humans.

References

- Reduan Achtabat, Maximilian Dreyer, Ilona Eisenbraun, Sebastian Bosse, Thomas Wiegand, Wojciech Samek, and Sebastian Lapuschkin. From” where” to” what”: Towards human-understandable explanations through concept relevance propagation. *arXiv preprint arXiv:2206.03208*, 2022.
- Matthew Barker, Katherine M Collins, Krishnamurthy Dvijotham, Adrian Weller, and Umang Bhatt. Selective concept models: Permitting stakeholder customisation at test-time. *arXiv preprint arXiv:2306.08424*, 2023.
- David Bau, Bolei Zhou, Aditya Khosla, Aude Oliva, and Antonio Torralba. Network dissection: Quantifying interpretability of deep visual representations. In *Proceedings of the IEEE conference on computer vision and pattern recognition*, pages 6541–6549, 2017a.
- David Bau, Bolei Zhou, Aditya Khosla, Aude Oliva, and Antonio Torralba. Network dissection: Quantifying interpretability of deep visual representations. In *Proceedings of the IEEE conference on computer vision and pattern recognition*, pages 6541–6549, 2017b.
- Eli Bingham, Jonathan P. Chen, Martin Jankowiak, Fritz Obermeyer, Neeraj Pradhan, Theofanis Karaletsos, Rohit Singh, Paul A. Szerlip, Paul Horsfall, and Noah D. Goodman. Pyro: Deep universal probabilistic programming. *J. Mach. Learn. Res.*, 20:28:1–28:6, 2019. URL <http://jmlr.org/papers/v20/18-403.html>.
- Xianjie Chen, Roozbeh Mottaghi, Xiaobai Liu, Sanja Fidler, Raquel Urtasun, and Alan Yuille. Detect what you can: Detecting and representing objects using holistic models and body parts. In *Proceedings of the IEEE conference on computer vision and pattern recognition*, pages 1971–1978, 2014.
- Jihye Choi, Jayaram Raghuram, Ryan Feng, Jiefeng Chen, Somesh Jha, and Atul Prakash. Concept-based explanations for out-of-distribution detectors. In *International Conference on Machine Learning*, pages 5817–5837. PMLR, 2023.
- Adam Coates, Andrew Ng, and Honglak Lee. An analysis of single-layer networks in unsupervised feature learning. In *Proceedings of the fourteenth international conference on artificial intelligence and statistics*, pages 215–223. JMLR Workshop and Conference Proceedings, 2011.
- Katherine Maeve Collins, Matthew Barker, Mateo Espinosa Zarlenga, Naveen Raman, Umang Bhatt, Mateja Jamnik, Ilia Sucholutsky, Adrian Weller, and Krishnamurthy Dvijotham. Human uncertainty in concept-based ai systems. In *Proceedings of the 2023 AAAI/ACM Conference on AI, Ethics, and Society*, pages 869–889, 2023.
- Mateo Espinosa Zarlenga, Pietro Barbiero, Gabriele Ciravegna, Giuseppe Marra, Francesco Gianini, Michelangelo Diligenti, Zohreh Shams, Frederic Precioso, Stefano Melacci, Adrian Weller, et al. Concept embedding models: Beyond the accuracy-explainability trade-off. *Advances in Neural Information Processing Systems*, 35:21400–21413, 2022.
- Amirata Ghorbani, James Wexler, James Y Zou, and Been Kim. Towards automatic concept-based explanations. *Advances in neural information processing systems*, 32, 2019.
- Zhi Huang, Federico Bianchi, Mert Yuksekgonul, Thomas J Montine, and James Zou. A visual-language foundation model for pathology image analysis using medical twitter. *Nature medicine*, 29(9):2307–2316, 2023.
- Been Kim, Martin Wattenberg, Justin Gilmer, Carrie Cai, James Wexler, Fernanda Viegas, et al. Interpretability beyond feature attribution: Quantitative testing with concept activation vectors (tcav). In *International conference on machine learning*, pages 2668–2677. PMLR, 2018.
- Eunji Kim, Dahuin Jung, Sangha Park, Siwon Kim, and Sungroh Yoon. Probabilistic concept bottleneck models. *arXiv preprint arXiv:2306.01574*, 2023a.
- Sunnie SY Kim, Elizabeth Anne Watkins, Olga Russakovsky, Ruth Fong, and Andrés Monroy-Hernández. ” help me help the ai”: Understanding how explainability can support human-ai interaction. In *Proceedings of the 2023 CHI Conference on Human Factors in Computing Systems*, pages 1–17, 2023b.

- Pang Wei Koh and Percy Liang. Understanding black-box predictions via influence functions. In *International conference on machine learning*, pages 1885–1894. PMLR, 2017.
- Pang Wei Koh, Thao Nguyen, Yew Siang Tang, Stephen Mussmann, Emma Pierson, Been Kim, and Percy Liang. Concept bottleneck models. In *International Conference on Machine Learning*, pages 5338–5348. PMLR, 2020.
- Mazda Moayeri, Keivan Rezaei, Maziar Sanjabi, and Soheil Feizi. Text-to-concept (and back) via cross-model alignment. *arXiv preprint arXiv:2305.06386*, 2023.
- Tuomas Oikarinen, Subhro Das, Lam M. Nguyen, and Tsui-Wei Weng. Label-free concept bottleneck models. In *International Conference on Learning Representations*, 2023. URL <https://openreview.net/forum?id=FlCg47MNvBA>.
- Alec Radford, Jong Wook Kim, Chris Hallacy, Aditya Ramesh, Gabriel Goh, Sandhini Agarwal, Girish Sastry, Amanda Askell, Pamela Mishkin, Jack Clark, et al. Learning transferable visual models from natural language supervision. In *International conference on machine learning*, pages 8748–8763. PMLR, 2021.
- Vikram V Ramaswamy, Sunnie SY Kim, Ruth Fong, and Olga Russakovsky. Overlooked factors in concept-based explanations: Dataset choice, concept salience, and human capability. *arXiv preprint arXiv:2207.09615*, 2022a.
- Vikram V Ramaswamy, Sunnie SY Kim, Nicole Meister, Ruth Fong, and Olga Russakovsky. Elude: Generating interpretable explanations via a decomposition into labelled and unlabelled features. *arXiv preprint arXiv:2206.07690*, 2022b.
- Marco Tulio Ribeiro, Sameer Singh, and Carlos Guestrin. ” why should i trust you?” explaining the predictions of any classifier. In *Proceedings of the 22nd ACM SIGKDD international conference on knowledge discovery and data mining*, pages 1135–1144, 2016.
- Russ Salakhutdinov. Statistical machine learning, 2011. URL <https://www.utstat.toronto.edu/~rsalakhu/sta4273/notes/Lecture2.pdf#page=10>.
- Ramprasaath R Selvaraju, Michael Cogswell, Abhishek Das, Ramakrishna Vedantam, Devi Parikh, and Dhruv Batra. Grad-cam: Visual explanations from deep networks via gradient-based localization. In *Proceedings of the IEEE international conference on computer vision*, pages 618–626, 2017.
- Sahil Singla and Soheil Feizi. Salient imagenet: How to discover spurious features in deep learning? In *International Conference on Learning Representations*, 2022. URL <https://openreview.net/forum?id=XVPqLYNxSyh>.
- Catherine Wah, Steve Branson, Peter Welinder, Pietro Perona, and Serge Belongie. The caltech-ucsd birds-200-2011 dataset. 2011.
- Wikipedia. Cosine similarity — Wikipedia, the free encyclopedia. <http://en.wikipedia.org/w/index.php?title=Cosine%20similarity&oldid=1178409159>, 2023a. [Online; accessed 18-November-2023].
- Wikipedia. Kendall tau distance — Wikipedia, the free encyclopedia. <http://en.wikipedia.org/w/index.php?title=Kendall%20tau%20distance&oldid=1163706720>, 2023b. [Online; accessed 25-September-2023].
- Wikipedia. Ordinary least squares — Wikipedia, the free encyclopedia. <http://en.wikipedia.org/w/index.php?title=Ordinary%20least%20squares>, Feb 2024. URL https://en.wikipedia.org/wiki/Ordinary_least_squares.
- Zhengxuan Wu, Karel D’Oosterlinck, Atticus Geiger, Amir Zur, and Christopher Potts. Causal proxy models for concept-based model explanations. In *International Conference on Machine Learning*, pages 37313–37334. PMLR, 2023.
- Chih-Kuan Yeh, Been Kim, and Pradeep Ravikumar. Human-centered concept explanations for neural networks. *arXiv preprint arXiv:2202.12451*, 2022.

- Mert Yuksekgonul, Maggie Wang, and James Zou. Post-hoc concept bottleneck models. *arXiv preprint arXiv:2205.15480*, 2022.
- Bolei Zhou, Agata Lapedriza, Aditya Khosla, Aude Oliva, and Antonio Torralba. Places: A 10 million image database for scene recognition. *IEEE Transactions on Pattern Analysis and Machine Intelligence*, 2017a.
- Bolei Zhou, Hang Zhao, Xavier Puig, Sanja Fidler, Adela Barriuso, and Antonio Torralba. Scene parsing through ade20k dataset. In *Proceedings of the IEEE conference on computer vision and pattern recognition*, pages 633–641, 2017b.
- Bolei Zhou, Yiyou Sun, David Bau, and Antonio Torralba. Interpretable basis decomposition for visual explanation. In *Proceedings of the European Conference on Computer Vision (ECCV)*, pages 119–134, 2018.

A Miscellaneous

A.1 Derivation of posterior on weights

The result of posterior distribution of weights follows directly from the form of posterior under normal prior on weights as explained as Salakhutdinov [2011] (Slide 10). For the sake of completeness, we also derive the result below.

$$\begin{aligned}
\Pr(\vec{w} \mid C_X, Y) &\propto \Pr(Y \mid C_X, \vec{w}) \Pr(\vec{w}) \\
&= \mathcal{N}(Y; C_X^T \vec{w}, \beta^{-1}) \mathcal{N}(\vec{w}; 0, S_0) \text{ where } S_0^{-1} = \lambda^{-1} \text{diag}(\epsilon \epsilon^T) \\
&\propto \exp \left\{ -\frac{\beta}{2} (Y - C_X^T \vec{w})^T (Y - C_X^T \vec{w}) - \frac{1}{2} \vec{w}^T S_0^{-1} \vec{w} \right\} \\
&\propto \exp \left\{ -\frac{1}{2} \vec{w}^T [\beta C_X C_X^T + S_0^{-1}] \vec{w} - \beta (C_X Y)^T \vec{w} \right\}
\end{aligned}$$

We see that the posterior also takes the form of normal distribution with $\Sigma^{-1} = \beta C_X C_X^T + S_0^{-1}$ and $\mu = \beta \Sigma C_X Y$.

A.2 Algorithm

We describe the algorithm summarizing U-ACE in 1. An additional technical detail of the algorithm is a step to sparsify weights as described below.

Sparsifying weights for interpretability. As a dense weight matrix can be hard to interpret, we induce sparsity in W_c by setting all the values below a threshold to zero. We pick the threshold such that the accuracy on train split does not fall by more than κ , which is a positive hyperparameter.

Algorithm 1: Uncertainty-Aware Concept Explanations (U-ACE)

Require: $\mathcal{D} = \{\mathbf{x}_1, \mathbf{x}_2, \dots, \mathbf{x}_N\}$, $\mathcal{T} = \{T_1, T_2, \dots, T_K\}$, f (model-to-be-explained), g (CLIP), κ

for $y = 1, \dots, L$ **do**

$Y = [f(\mathbf{x})[y] \text{ for } \mathbf{x} \in \mathcal{D}^T]$ ▷ Gather logits

$C_X = [\vec{m}(\mathbf{x}_1), \dots, \vec{m}(\mathbf{x}_N)]$, $\epsilon = \mathbb{E}_{\mathcal{D}}[\vec{s}(\mathbf{x})]$ ▷ Estimate $\vec{m}(\mathbf{x})$, $\vec{s}(\mathbf{x})$ (Section 3.1)

$\vec{w}_y \sim \mathcal{N}(\mu_y, \Sigma_y)$ where μ_y, Σ_y from Equation 1 ▷ Estimate λ, β using MLL

end for

$W_c = \text{sparsify}([\vec{\mu}_1, \vec{\mu}_2, \dots, \vec{\mu}_L], \kappa)$ ▷ Suppress less useful weights, Section 3

return $W_c, [\text{diag}(\Sigma_1), \text{diag}(\Sigma_2), \dots, \text{diag}(\Sigma_L)]$

B Maximum Likelihood Estimation of U-ACE parameters

The posterior on weights shown in Equation 1 has two parameters: λ, β as shown below with C_X and Y are array of concept activations and logit scores (see Algorithm 1).

$$\vec{w} \sim \mathcal{N}(\mu, \Sigma) \quad \text{where } \mu = \beta \Sigma C_X Y, \quad \Sigma^{-1} = \beta C_X C_X^T + \lambda^{-1} \text{diag}(\epsilon \epsilon^T)$$

We obtain the best values of λ and β that maximize the log-likelihood objective shown below.

$$\lambda^*, \beta^* = \arg \max_{\lambda, \beta} \mathbb{E}_Z \left[-\frac{\beta^2 \|Y - (C_X + Z)^T \vec{w}(\lambda, \beta)\|^2}{2} + \log(\beta) \right]$$

where Z is uniformly distributed in the range given by error intervals

$$Z \sim \text{Unif}([-\vec{s}(\mathbf{x}_1), -\vec{s}(\mathbf{x}_2), \dots], [\vec{s}(\mathbf{x}_1), \vec{s}(\mathbf{x}_2), \dots])$$

We implement the objective using Pyro software library [Bingham et al., 2019] and Adam optimizer.

C Proof of Proposition 1

We restate the result for clarity.

For a concept k and $\cos(\alpha_k)$ defined as $\cos\text{-sim}(e(v_k, f, \mathcal{D}), e(w_k, g, \mathcal{D}))$, we have the following

result when concept activations in f for an instance \mathbf{x} are computed as $\cos\text{-sim}(f(\mathbf{x}), v_k)$ instead of $v_k^T f(\mathbf{x})$.

$$\vec{m}(\mathbf{x})_k = \cos(\theta_k)\cos(\alpha_k), \quad \vec{s}(\mathbf{x})_k = \sin(\theta_k)\sin(\alpha_k)$$

where $\cos(\theta_k) = \cos\text{-sim}(g_{\text{text}}(T_k), g(\mathbf{x}))$ and $\vec{m}(\mathbf{x})_k, \vec{s}(\mathbf{x})_k$ denote the k^{th} element of the vector.

Proof. Corresponding to v_k in f , we assume there is an equivalent vector w in the embedding space of g such that $\cos\text{-sim}(f(\mathbf{x}), v_k) = \cos\text{-sim}(g(\mathbf{x}), w)$ for any \mathbf{x} . For example, the assumption is met when there is a linear mapping between $f(\mathbf{x}) \approx Wg(\mathbf{x})$ [Moayeri et al., 2023] for a unitary matrix ($W^T W = I$), in which case w is simply Wv_k . For such a w , the following condition on $\cos(\alpha_k)$ must hold as well.

$$\cos(\alpha_k) = \cos\text{-sim}(e(v_k, f, \mathcal{D}), e(w_k, g, \mathcal{D})) = \cos\text{-sim}(e(w, g, \mathcal{D}), e(w_k, g, \mathcal{D}))$$

Denote the matrix of vectors embedded using g by $G = [g(\mathbf{x}_1), g(\mathbf{x}_2), \dots, g(\mathbf{x}_N)]^T$ a $N \times D$ matrix (D is the dimension of g embeddings). Let U be a matrix with S basis vectors of size $S \times D$. We can express each vector as a combination of basis vectors and therefore $G = AU$ for a $N \times S$ matrix A .

Substituting the terms in the $\cos\text{-sim}$ expression, we have:

$$\begin{aligned} \cos(\alpha_k) &= \cos\text{-sim}(Gw, Gw_k) = \cos\text{-sim}(AUw, AUw_k) \\ &= \frac{w^T U^T A^T AUw_k}{\sqrt{(w^T U^T A^T AUw)(w_k^T U^T A^T AUw_k)}}. \end{aligned}$$

If the examples in \mathcal{D} are diversely distributed without any systematic bias, $A^T A$ is proportional to the identity matrix, meaning the basis of G and W are effectively the same. We therefore have $\cos(\alpha_k) = \cos\text{-sim}(Gw, Gw_k) = \cos\text{-sim}(Uw, Uw_k)$, i.e. the projection of w, w_k on the subspace spanned by the embeddings have $\cos(\alpha_k)$ cosine similarity. Since w, w_k are two vectors that are α_k apart, an arbitrary new example \mathbf{x} that is at an angle of θ from w_k is at an angle of $\theta \pm \alpha_k$ from w . The cosine similarity follows as below.

$$\begin{aligned} \cos(\theta) &= \cos\text{-sim}(w_k, g(\mathbf{x})) \implies \cos\text{-sim}(w, g(\mathbf{x})) = \cos(\theta \pm \alpha_k) \\ &= \cos(\theta)\cos(\alpha_k) \pm \sin(\theta)\sin(\alpha_k) \end{aligned}$$

Because w is a vector in g corresponding to v_k in f , $\cos\text{-sim}(w, g(\mathbf{x})) = \cos\text{-sim}(v_k, f(\mathbf{x}))$. \square

D Proof of Proposition 2

The concept importance estimated by U-ACE when the input dimension is sufficiently large and for some $\lambda > 0$ is approximately given by $v_k = \frac{\mathbf{u}_k^T \mathbf{w}}{\mathbf{u}_k^T \mathbf{u}_k + \lambda \sigma_k^2}$. On the other hand, the importance scores estimated using vanilla linear estimator under the same conditions is distributed as $v_k \sim \mathcal{N}(\frac{\mathbf{u}_k^T \mathbf{w}}{\mathbf{u}_k^T \mathbf{u}_k}, \sigma_k^2 \frac{\|\mathbf{w}\|^2}{\|\mathbf{u}_k\|^2})$.

Proof. We use the known result that inner product of two random vectors is close to 0 when the number of dimensions is large, i.e. $\mathbf{u}_i^T \mathbf{u}_j \approx 0, i \neq j$.

Solution with standard estimator. We first show the solution using vanilla estimator is distributed as given by the result above. We wish to estimate v_1, v_2, \dots such that we approximate the prediction of model-to-be-explained: $y = \mathbf{w}^T \mathbf{x}$. We denote by \mathbf{w}_k sampled from the normal distribution of concept vectors. We require $w^T \mathbf{x} \approx \sum_k v_k \mathbf{w}_k^T \mathbf{x}$. In effect, we are optimising for v_k such that $\|\mathbf{w} - \sum_k v_k \mathbf{w}_k\|^2$ is minimized. We multiply the objective by \mathbf{u}_k and use the result that random vectors are almost orthogonal in high-dimensions to arrive at objective $\arg \min_{v_k} \|\mathbf{w}_k^T \mathbf{w} - v_k (\mathbf{w}_k^T \mathbf{w}_k)\|$. Which is minimized trivially when $v_k = \frac{\mathbf{w}_k^T \mathbf{w}}{\|\mathbf{w}_k\|^2}$. Since \mathbf{w}_k is normally distributed with $\mathcal{N}(\mathbf{u}_k, \sigma_k^2 I)$, $\mathbf{w}_k^T \mathbf{w} = (\mathbf{u}_k + \vec{\epsilon})^T \mathbf{w}$, $\vec{\epsilon} \sim \mathcal{N}(0, I)$ is also normally distributed with $\mathcal{N}(\mathbf{u}_k^T \mathbf{w}, \sigma_k^2 \|\mathbf{w}\|^2)$. We approximate the denominator with its average and ignoring its variance, i.e. $\|\mathbf{w}_k\|^2 = \mathcal{N}(\|\mathbf{u}_k\|^2, \sigma_k^2) \approx \|\mathbf{u}_k\|^2$ which is when $\|\mathbf{u}_k\|^2 \gg \sigma^2$. We therefore have the result that v_k is normally distributed with mean $\frac{\mathbf{u}_k^T \mathbf{w}}{\|\mathbf{u}_k\|^2}$ and variance $\sigma_k^2 \frac{\|\mathbf{w}\|^2}{\|\mathbf{u}_k\|^2}$.

Solution with U-ACE. Unlike the standard estimator, U-ACE seeks a solution by first estimating the distribution on concept activations. We make an approximation of our proposed estimation of U-ACE and find a solution using the following objective, recall that the k^{th} activation vector is defined to have been sampled from $\mathcal{N}(\mathbf{u}_k, \sigma_k^2 I)$.

$$\ell = \arg \min_v \{ \|\mathbf{w} - \sum_k v_k \mathbf{u}_k\|^2 + \lambda \sum_k \sigma_k^2 v_k^2 \}$$

With sufficient number of examples, the mean and variance \mathbf{u}_k, σ^2 can be faithfully estimated. The above objective captures the essence of U-ACE (Eqn. (1)) because (1) it fits the observations, and (2) regularizes importance of concepts with high variance. We now proceed with finding the closed form solution of v_k .

$$\ell = \arg \min_v \{ \|\mathbf{w} - \sum_k v_k \mathbf{u}_k\|^2 + \lambda \sum_k \sigma_k^2 v_k^2 \}$$

setting $\frac{\partial \ell}{\partial v_k} = 0$ we obtain

$$-\mathbf{u}_k^T (\mathbf{w} - \sum_j v_j \mathbf{u}_j) + \lambda \sigma_k^2 v_k = 0$$

and using almost zero inner product result stated above, i.e. $\mathbf{u}_i^T \mathbf{u}_j \approx 0, i \neq j$, we get

$$\Rightarrow v_k = \frac{\mathbf{u}_k^T \mathbf{w}}{\|\mathbf{u}_k\|^2 + \lambda \sigma_k^2}$$

□

E Corollary of Proposition 2

Following the result of Proposition 2, we have the following result on the v_k estimated by U-ACE and the standard linear estimator.

Corollary 2. *For the data setup of Proposition 2, the following results holds when $\mathbf{u}_1 = \mathbf{w}, \sigma_1 \approx 0$ and $\mathbf{u}_k^T \mathbf{w} = 0, \forall k \in [2, K]$. Then the probability that the standard estimator returns the first concept as the most salient decreases exponentially with the number of concepts. On the other hand, the importance score assigned by U-ACE is 1 for the only relevant first concept and 0 otherwise.*

Proof. Plugging in the values for the special case of $\mathbf{u}_1 = \mathbf{w}, \sigma_1 \approx 0$ and $\mathbf{u}_k^T \mathbf{w} = 0, k \geq 2$ in the closed form solution from Proposition 2, we have the following results for the standard linear estimator and U-ACE.

Solution of standard estimator. $v_1 = 1$ and $v_k \sim \mathcal{N}(0, \sigma_k^2 \frac{\|\mathbf{w}\|^2}{\|\mathbf{u}_k\|^2})$ for $k \geq 2$.

For the first concept to remain the most salient, rest of the $K-1$ concepts must have an importance score less than 1. Recall that the probability that a random variable $z \sim \mathcal{N}(\mu, \sigma^2)$ less than a value z_0 is $\Phi(\frac{z_0 - \mu}{\sigma})$ where Φ is the Cumulative Distribution Function of a standard normal distribution. Therefore the probability that all the $K-1$ concepts having a value less than 1 is $\prod_{k=2}^K \Phi(\frac{1-0}{\sigma_k \|\mathbf{w}\| / \|\mathbf{u}_k\|}) = \prod_{k=2}^K \Phi(\frac{\|\mathbf{u}_k\|}{\sigma_k \|\mathbf{w}\|})$. Since the probability is a product over $K-1$ quantities, it decreases exponentially with K .

Solution of U-ACE. $v_1 = 1, v_2, v_3, \dots = 0$ follows directly from plugging in the values in to result of the proposition.

□

F Proof of Proposition 3

The importance score estimated by U-ACE is approximately $\frac{b_1/2}{1+\lambda\sigma^2}, \frac{b_2/2}{1+\lambda\sigma^2}$, where $\lambda > 0$ is a regularizing hyperparameter.

Proof. Since β_1, β_2 are normal distributed, the concept activation vectors $\beta_1 \mathbf{u} + (1 - \beta_1) \mathbf{v}$ and $\beta_2 \mathbf{u} + (1 - \beta_2) \mathbf{v}$ are also normally distributed. We derive their closed form below. Recall that $\beta_1 \sim \mathcal{N}(b_1, \sigma^2)$, $\beta_2 \sim \mathcal{N}(b_2, \sigma^2)$ and that \mathbf{u}, \mathbf{v} are orthogonal and unit vectors.

$$\begin{aligned}\mathbb{E}[\beta_1 \mathbf{u} + (1 - \beta_1) \mathbf{v}] &= b_1 \mathbf{u} + (1 - b_1) \mathbf{v} \\ \mathbb{V}[\beta_1 \mathbf{u} + (1 - \beta_1) \mathbf{v}] &= \mathbb{E}[(\beta_1 - b_1) \mathbf{u} + (b_1 - \beta_2) \mathbf{v}]^2 \\ &= \mathbb{E}[(\beta_1 - b_1)^2] + \mathbb{E}[(\beta_2 - b_2)^2] \\ &= 2\sigma^2\end{aligned}$$

As argued of the objective to approximate U-ACE in Appendix D, we may obtain the closed form solution for the concept scores η_1, η_2 by solving the following objective.

$$\ell = \|\mathbf{u} - \eta_1(b_1 \mathbf{u} + (1 - b_1) \mathbf{v}) - \eta_2(b_2 \mathbf{u} + (1 - b_2) \mathbf{v})\|^2 + 2\lambda\sigma^2(\eta_1^2 + \eta_2^2)$$

By setting $\partial\ell/\partial\eta_1 = 0$, $\partial\ell/\partial\eta_2 = 0$, and simplifying, we get the following.

$$\begin{aligned}b_1 &= \eta_1(b_1^2 + (1 - b_1)^2 + 2\lambda\sigma^2) + \eta_2(b_1 b_2 + (1 - b_1)(1 - b_2)) \\ b_2 &= \eta_2(b_2^2 + (1 - b_2)^2 + 2\lambda\sigma^2) + \eta_1(b_1 b_2 + (1 - b_1)(1 - b_2))\end{aligned}$$

Eliminating variables, and solving for η_1 , we get

$$\eta_1 = \frac{2\lambda b_1 \sigma^2 + (1 - b_2)(b_1 - b_2)}{(b_1 - b_2)(b_1 + b_2 - 2b_1 b_2) + 2\lambda\sigma^2(2\lambda\sigma^2 + b_1^2 + b_2^2 + (1 - b_1)^2 + (1 - b_2)^2)} = \text{similarly for } \eta_2$$

By substituting $b_1 - b_2 \approx 0$, the expressin can be simplified as

$$\eta_1 = \frac{b_1}{2\lambda\sigma^2 + b_1^2 + b_2^2 + (1 - b_1)^2 + (1 - b_2)^2}$$

If we now use the assumption that $b_1, b_2 \approx 0$, $\therefore 1 - b_1, 1 - b_2 \approx 1$, we get the final form below.

$$\begin{aligned}\eta_1 &= \frac{b_1}{2(1 + \lambda\sigma^2)} \\ \eta_2 &= \frac{b_2}{2(1 + \lambda\sigma^2)}\end{aligned}$$

□

Solution of standard estimator.

When $c_1^{(i)} = (\beta_1 u + (1 - \beta_1) v)^T z^{(i)}$, $c_2^{(i)} = (\beta_2 u + (1 - \beta_2) v)^T z^{(i)}$ we can derive the value of the label by their scaled difference as shown below

$$\begin{aligned}\frac{(1 - \beta_2)c_1^{(i)} - (1 - \beta_1)c_2^{(i)}}{(1 - \beta_2)\beta_1 - (1 - \beta_1)\beta_2} &= \frac{(1 - \beta_2)c_1^{(i)} - (1 - \beta_1)c_2^{(i)}}{\beta_1 - \beta_2} = u^T z^{(i)} = y^{(i)} \\ \implies \frac{1 - \beta_2}{\beta_1 - \beta_2} c_1^{(i)} + \frac{1 - \beta_1}{\beta_1 - \beta_2} c_2^{(i)} &= y_i \\ \implies v_1 = \frac{1 - \beta_2}{\beta_1 - \beta_2}, v_2 = \frac{1 - \beta_1}{\beta_1 - \beta_2}\end{aligned}$$

G Additional experiment details

G.1 Simulated Study

In this section, we consider explaining a two-layer CNN model trained to classify between solid color images with pixel noise as shown in Figure 4. The colors on the left (red; green) are defined as label 0 and the colors on the right (blue; white) are defined as label 1.

The model-to-be-explained is trained on a dataset with equal proportion of all colors; we therefore expect that all constituent colors of a label are equally important for the label. We specify a concept set with the four colors encoded by their literal name *red*, *green*, *blue*, *white*. U-ACE (along with others) attribute positive importance for *red*, *green* and negative or zero importance for *blue*, *white* when explaining label 0 using a concept set with only the four task-relevant concepts and when the probe-dataset is the same distribution as the training dataset. However, quality of explanations quickly degrades when the probe-dataset is shifted, or if the concept set is misspecified.

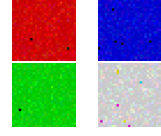


Figure 4: Toy

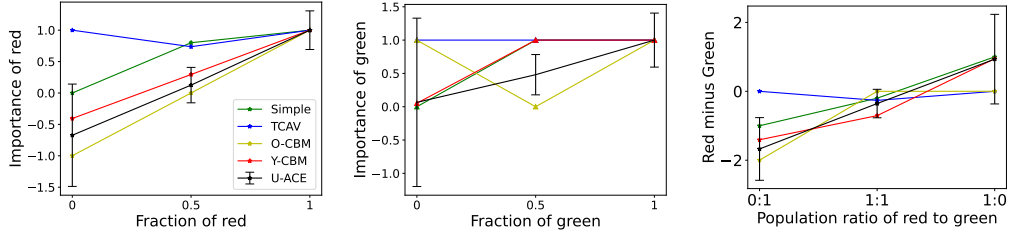


Figure 5: Left, middle plots show the importance of red and green concepts while the rightmost plot shows their importance score difference. U-ACE estimated large uncertainty in importance score when red or green concept is missing from the dataset as seen in the left of the left and middle plots. Also the difference in importance at either extreme in the right plot is not statistically significant.

Unreliability due to dataset shift. We varied the probe-dataset to include varying populations of colors while keeping the concept set and model-to-be-explained fixed. We observed that importance of a concept estimated with standard CBEs varied with the choice of probe-dataset for the same underlying model-to-be-explained as shown in left and middle plots of Figure 5. Most methods attributed incorrect importance to the *red* concept when it is missing (left extreme of left plot), and similarly for the *green* concept (left extreme of middle plot). Such explanations would have led the user to believe that *green* is more important than *red*, or *red* is more important than *green*, depending on the probe-dataset used (as shown in the right most plot). In practice, mis-communicated concept importance could be disastrous, if such importances are used to inform decision making and/or discovery. Because U-ACE also informs the user of uncertainty in the estimated importance, we see that the difference in importance scores between the two colors at either extremes is not statistically significant as shown in the rightmost plot.

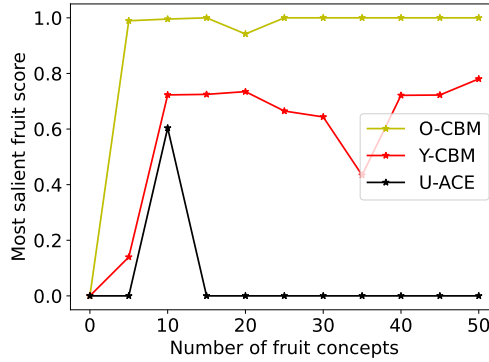


Figure 6: U-ACE is reliable even with overly complete concept set.

Over-complete concept set. We now evaluate the quality of explanations when the concept set is misspecified. We induce misspecification by making the concept set over-complete by gradually expanding it to include common fruit names (Appendix G contains the full list), which are clearly irrelevant to the task. We obtain the explanations using an in-distribution probe-dataset that contains all colors in equal proportion. Figure 6 shows the score of most salient fruit concept with increasing number of fruit (nuisance) concepts on X-axis. We observe that U-ACE is far more robust to the

presence of nuisance concepts. Robustness to irrelevant concepts is important because it allows the user to begin with a superfluous set of concepts and find their relevance to model-to-be-explained, instead of requiring users to guess relevant concepts, which is ironically the very purpose of using concept explanations.

Under-complete concept set. We now generate concept explanations with concepts set to {“*red or blue*”, “*blue or red*”, “*green or blue*”, “*blue or green*”}. The concept “*red or blue*” is expected to be active for both *red* or *blue* colors, similarly for “*blue or red*” concept. Since all the concepts contain a color from each label, i.e. are active for both the labels, none of them must be useful for prediction. Yet, the importance scores estimated by Y-CBM and O-CBM shown in the Figure 5 table attribute significant importance. U-ACE avoids this problem as explained in Section 3.2 and attributes almost zero importance.

Concept	Y-CBM	O-CBM	U-ACE
red or blue	-75.4	-1.8	0.1
blue or red	21.9	-1.9	0
green or blue	-1.4	1.6	0
blue or green	-23.1	1.6	0

Table 5: When the concept set is under-complete and contains only nuisance concepts, their estimated importance score must be 0.

List of fruit concepts from Section G.1.

apple, apricot, avocado, banana, blackberry, blueberry, cantaloupe, cherry, coconut, cranberry, cucumber, currant, date, dragonfruit, durian, elderberry, fig, grape, grapefruit, guava, honeydew, kiwi, lemon, lime, loquat, lychee, mandarin orange, mango, melon, nectarine, orange, papaya, passion fruit, peach, pear, persimmon, pineapple, plum, pomegranate, pomelo, prune, quince, raspberry, rhubarb, star fruit, strawberry, tangerine, tomato, watermelon

List of animal concepts from Section 5.

lion, tiger, giraffe, zebra, monkey, bear, wolf, fox, dog, cat, horse, cow, pig, sheep, goat, deer, rabbit, raccoon, squirrel, mouse, rat, snake, crocodile, alligator, turtle, tortoise, lizard, chameleon, iguana, komodo dragon, frog, toad, turtle, tortoise, leopard, cheetah, jaguar, hyena, wildebeest, gnu, bison, antelope, gazelle, gemsbok, oryx, warthog, hippopotamus, rhinoceros, elephant seal, polar bear, penguin, flamingo, ostrich, emu, cassowary, kiwi, koala, wombat, platypus, echidna, elephant

Concepts used for *car* and *plane* from Section 5

car: headlights, taillights, turn signals, windshield, windshield wipers, bumpers, wheels
plane: wings, landing gear, sky

Scene labels considered in Section 6.1.

/a/arena/hockey, /a/auto_showroom, /b/bedroom, /c/conference_room, /c/corn_field
/h/hardware_store, /l/legislative_chamber, /t/tree_farm, /c/coast,
/p/parking_lot, /p/pasture, /p/patio, /f/farm, /p/playground, /f/field/wild
/p/playroom, /f/forest_path, /g/garage/indoor
/g/garage/outdoor, /r/runway, /h/harbor, /h/highway
/b/beach, /h/home_office, /h/home_theater, /s/slum,
/b/berth, /s/stable, /b/boat_deck, /b/bow_window/indoor,
/s/street, /s/subway_station/platform, /b/bus_station/indoor, /t/television_room,
/k/kennel/outdoor, /c/campsite, /l/lawn, /t/tundra, /l/living_room,

/l/loading_dock, /m/marsh, /w/waiting_room, /c/computer_room,
/w/watering_hole, /y/yard, /n/nursery, /o/office, /d/dining_room, /d/dorm_room,
/d/driveway

G.2 Further details for Imagenet experiment of Section 6.2

Table 6 contains the list of labels we considered for evaluation on the Imagenet dataset of Section 6.2.

Table 7 extends with more results the Table 4 of the main content.

Index	Name	Known spurious features
1	dogsled	snow, dog, tree, trees, husky
2	howler monkey	trunk, green, branches, branch, vegetation
3	seat belt, seatbelt	passenger, window, sunglasses, van
4	ski	tree, trees, snow, mountain, person, sunglasses
5	volleyball	sand, players, player, setter, scoreboard, net
6	boathouse	lake, water, dock, boat, shore
7	bee	flower, daisy, petals
8	plate	food, table, dining
9	barracouta, snoek	person, face, hands, hand, sunglasses, cap
10	llama	hay, grass, green, greens
11	rhinoceros beetle	hand, head, palm, person, fingers
12	dowitcher	water, reflection, lake, shoal, sandbar
13	white wolf, Arctic wolf	net, fence, fencing
14	dragonfly	blurry, green, flower, plant
15	gorilla, Gorilla gorilla	green, tree, grass, trunk
16	shovel	snow
17	doormat, welcome mat	door
18	ruddy turnstone, Arenaria interpres	mud, shore, sand, land, seashore, beach
19	albatross, mollymawk	water, sea, ocean
20	sax, saxophone	player, players, playing
21	balance beam, beam	player, person, sport, arms, legs
22	bathing cap, swimming cap	face, chest, person, swimmer, diver, gymnast
23	puck, hockey puck	player, bat, ice, arena
24	dining table, board	chairs, chair, corner
25	rugby ball	ground, green, players, player
26	dock, dockage, docking facility	boat, boats, ship, yacht, water, sea, lake
27	padlock	chain, chains, door
28	potter's wheel	hands, hand, person, face, head
29	ping-pong ball	player, human, hands, arms, arm
30	paddle, boat paddle	human, arm, arms, body, lifevest, water
31	unicycle, monocycle	road, body, human, arms, face, arm
32	ice lolly, lolly, lollipop, popsicle	mouth, eyes, face, human, head, hand, lip, lips
33	beaver	water, lake, waterbody
34	mountain tent	mountain, lake, water, hill, snow
35	indri, indris, Indri indri, Indri brevicaudatus	sky, tree, leaf, leaves, trunk, vegetation, green
36	seashore, coast, seacoast, sea-coast	seawater, ocean, water, sea
37	sunglass	cheeks, face, head, person, nose
38	bulbul	branch, tree, leaves, sky, leaf
39	alp	sky, clouds, blue
40	Arabian camel	desert, sand, hot, water, ground

Table 6: Classes selected for evaluation in Section 6.2 and known spurious features in the last column. The known spurious features are obtained from Salient-Imagenet

G.3 Addition results for Section 6.1

We report also the tau [Wikipedia, 2023b] distance from concept explanations computed by *Oracle* as a measure of explanation quality in Table 8. Kendall Tau is a standard measure for measuring

volley ball	Y-CBM	setter, ball, airship
	O-CBM	setter, ball, clay
	U-ACE	sports, setter, ball
Gorilla	Y-CBM	animals, siamang, mower
	O-CBM	chimp, black, mastiff
	U-ACE	siamang, gibbon, macaque
Rugby ball	Y-CBM	rugby, knee, missile
	O-CBM	rugby, soccer, bulldog
	U-ACE	rugby, sports, player
hockey puck	Y-CBM	hockey, player, nail
	O-CBM	hockey, shaft , heater
	U-ACE	hockey, sports, gandola
swimming cap	Y-CBM	hat, regions , bandaid
	O-CBM	swimming, bald , meets
	U-ACE	swimming, sports, snorkel

Table 7: More results extending the Table 4

distance between two ranked lists. It does so by computing number of pairs with reversed order between any two lists. Since *Oracle* can only estimate the importance of concepts that are correctly annotated in the dataset, we restrict the comparison to only over concepts that are attributed non-zero importance by *Oracle*.

Dataset↓	TCAV	O-CBM	Y-CBM	U-ACE
ADE20K	0.36	0.48	0.48	0.34
PASCAL	0.46	0.52	0.52	0.32

Table 8: *Quality of explanation comparison.* Kendall Tau Distance between concept importance rankings computed using different explanation methods shown in the first row with ground-truth. The ranking distance is averaged over twenty labels. U-ACE is better than both Y-CBM and O-CBM as well as TCAV despite not having access to ground-truth concept annotations.

H Ablation Study

H.1 Uncertainty of Concept Activations

As explained in Section 3.1, we estimate the uncertainty on concept activations using a measure on predictability of the concept as shown in Proposition 1. In this section we evaluate the quality of estimated uncertainty and compare with other (simpler) variants of uncertainty estimation. More crisply, we ask the following question.

Why not estimate uncertainty using any other uncertainty quantification method?

We will now introduce two new variants of estimating uncertainty. Alongside the measure of uncertainty of U-ACE discussed in Section 3.1, which we denote with ϵ , we will present two alternate ways of measuring uncertainty below.

MC Sampling. We may simply repeat the estimation procedure several times (denote by S) with different seed and data split to sample multiple concept activation vectors: $\{a_k^{(1)}, a_k^{(2)}, \dots, a_k^{(S)}\}$ $k \in [1, K]$. We empirically estimate per-concept uncertainty by averaging over examples: $\epsilon^{MC} = \mathbb{E}_{\mathbf{x} \in \mathcal{D}}[V(\mathbf{x}^T a_k^{(1)}, \mathbf{x}^T a_k^{(2)}, \dots, \mathbf{x}^T a_k^{(S)})]$. Where $V(\bullet)$ is the sample variance: $V(b_1, b_2, \dots, b_S) = \frac{\sum_s (b_s - \frac{\sum_s b_s}{S})^2}{S-1}$. We simply repeated the estimation procedure of Oikarinen et al. [2023] that is summarized in Section 3.1 multiple times with different seed and data split to sample different activation vectors.

Distribution Fit. Inspired by ProbCBM proposed in Kim et al. [2023a], we estimate uncertainty from the data as a learnable parameter through distribution fitting. We assume a normal distribution of the noise and model the standard deviation as a linear projection of the feature vector. The model

is summarized below.

$$g(\mathbf{x})^T g_{text}(T_k) \sim \mathcal{N}(\mu_k(\mathbf{x}), \sigma_k^2(\mathbf{x}))$$

$$\mu_k(\mathbf{x}) = \vec{p}_k^T f(\mathbf{x}), \sigma_k(\mathbf{x}) = \vec{q}_k^T f(\mathbf{x})$$

We obtain the observed score of a concept given an example: \mathbf{x} using the multi-modal model: g, g_{text} and the text description of the k^{th} concept T_k . The concept score is modeled to be distributed by a normal distribution whose mean and standard deviation are linear functions of the feature representation of the model-to-be-explained: $f^{[-1]}(\mathbf{x})$. We optimize the value for $[\vec{p}_1, \vec{p}_2, \dots, \vec{p}_K], [\vec{q}_1, \vec{q}_2, \dots, \vec{q}_K]$ through gradient descent on the objective $\beta = MLL(\mathcal{D}, g) + \beta \times \mathbb{E}_{\mathcal{D}} \mathbb{E}_k [KL(\mathcal{N}(0, I) \| \mathcal{N}(\mu_k(\mathbf{x}), \sigma_k(\mathbf{x})))]$ very similar to the proposal of Kim et al. [2023a]. We picked the best value of β and obtained ϵ^{DF} by averaging over all the examples: $\epsilon^{DF} = \mathbb{E}_{\mathcal{D}}[\sigma_k(\mathbf{x})]$.

Evaluation of different uncertainties. We conduct our study using the ResNet-18 model pre-trained on Places365 and Pascal dataset that were discussed in Section 6.1. We use human-provided concept annotations to train per-concept linear classifier on the representation layer. We retained only 215 concepts of the total 720 concepts that have at least two positive examples in the dataset. We then evaluated the per-concept linear classifier on a held-out test set to obtain macro-averaged accuracy. The concepts with poor accuracy are the ones that cannot be classified linearly using the representations. Therefore the error rate per concept is the ground-truth for uncertainty that we wish to quantify.

We may now evaluate the goodness of uncertainty: ϵ of U-ACE by comparing it with ground-truth (error-rate); observe they are both K-dimensional vectors. We report two measures of similarity in Table 9: (1) Cosine-Similarity (Cos-Sim) between ϵ and error-rate, (2) Jaccard Similarity (JS) (https://en.wikipedia.org/wiki/Jaccard_index) between top-k least uncertain concepts identified using error-rate and ϵ . For any two vectors u, v , and their top-k sets: $S_1(u), S_2(v)$, the Cos-Sim and JS are evaluated as follows.

$$\text{Cos-Sim}(u, v) = \frac{u^T v}{\|u\| \|v\|}$$

$$\text{JS}(S_1(u), S_2(v)) = \frac{|S_1(u) \cap S_2(v)|}{|S_1(u) \cup S_2(v)|}$$

Evaluation of epistemic uncertainty. We compared the estimate of uncertainty obtained through MC sampling (ϵ^{MC} with hundred samples) and Distribution Fitting (ϵ^{DF}) with ϵ of U-ACE in Table 9. We observe that uncertainty obtained using distributional fitting is decent without incurring huge computational cost, however U-ACE produced the highest quality uncertainty at the same or slightly lower computational cost of distributional fitting.

Method	Cos-Sim	Top-10	Top-40	Top-80
MC Sampling	-0.13	0	0.08	0.21
Distribution Fit	0.06	0.11	0.19	0.31
U-ACE	0.36	0.11	0.29	0.36

Table 9: Evaluation of uncertainties estimated using U-ACE, MC sampling and Distribution Fit (see text for their description). Cos-Sim is the cosine-similarity with ground-truth value of uncertainty. The next three columns show Jaccard similarity between the top-k concepts ranked by ground-truth uncertainty and each of the three methods. Higher the better for all the values.

Evaluation of uncertainty due to ambiguity. The results so far have confirmed the merits of U-ACE over the other two in modelling the uncertainty due to lack of information. In Figures 7,8,9,10, we present anecdotal evidence that U-ACE is very effective at modelling uncertainty due to ambiguity. In each figure, we compare most (first two columns) and least (last two columns) uncertain images identified by Distribution Fit (in the first row) and U-ACE in the second row.

H.2 Bayesian Estimation and Significance of Prior

The focus of this section is to motivate the uncertainty-aware prior used by U-ACE. More crisply, the subject of this section is to answer the following question.

What is the role of prior in U-ACE, and what happens without it?

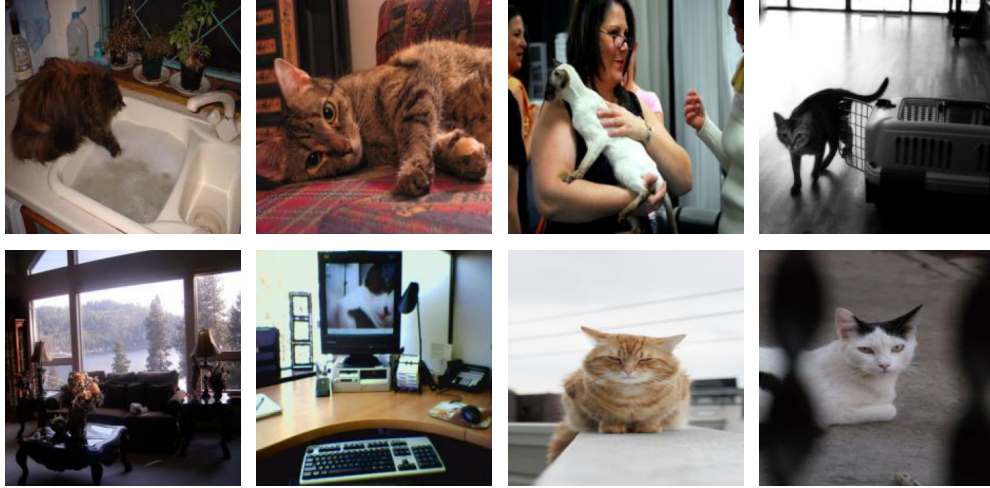


Figure 7: Comparison of ambiguity ranking for **Cat** with Distr. Fit in the top row and U-ACE in the bottom row. Most uncertainty (due to ambiguity) on the left to least uncertainty on the right.



Figure 8: Comparison of ambiguity ranking for **Bird** with Distr. Fit in the top row and U-ACE in the bottom row. Most uncertainty (due to ambiguity) on the left to least uncertainty on the right.

We replicate the study on Broden dataset of Section 6.1 of Table 1 with two new baselines. We replace the linear model estimation of U-ACE described in Section 3 with an out-of-the-box Bayesian Regression estimator available from `sklearn`², which we refer as Bayes Regr. Effectively, Bayes Regr. is different from U-ACE only in the prior. We also compare with the estimation of fitting using Bayes Regr. but when the input is perturbed with the noise estimated by U-ACE. We refer to this baseline as Bayes Regr. with MC.

Table 10 contrasts the two methods that differ majorly only on the choice of prior with U-ACE. We observe a drastic reduction in the quality of explanations by dropping the prior.

Can we trivially fix TCAV with a simple uncertainty estimate?

TCAV is already equipped with a simple uncertainty measurement to distinguish a truly important concept from a random concept. TCAV computes $m(\vec{x})$ and $s(\vec{x})$ of concept activations by simply training multiple concept activation vectors. Yet, TCAV estimated explanations are noisy as seen in Table 1 and in the top-10 salient concepts shown below. The poor quality of TCAV explanations

²https://scikit-learn.org/stable/modules/generated/sklearn.linear_model.BayesianRidge.html

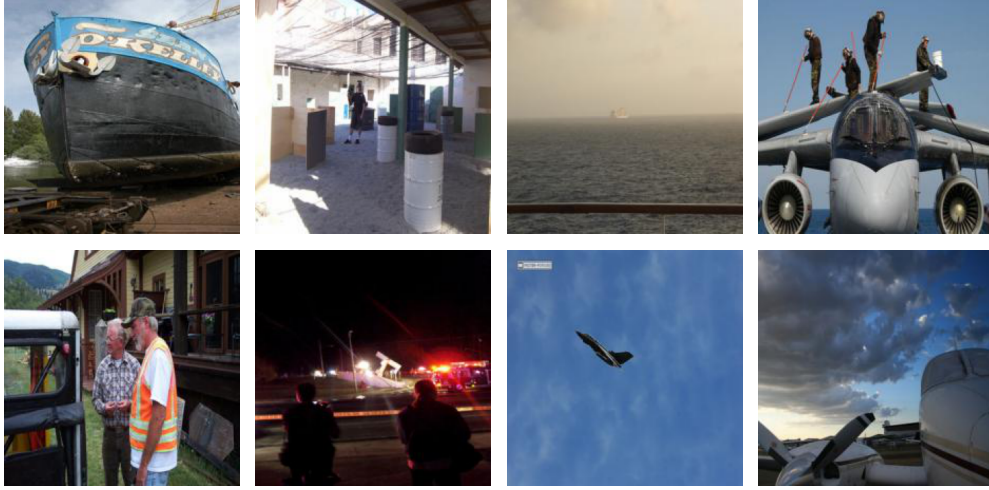


Figure 9: Comparison of ambiguity ranking for **Sky** with Distr. Fit in the top row and U-ACE in the bottom row. Most uncertainty (due to ambiguity) on the left to least uncertainty on the right.

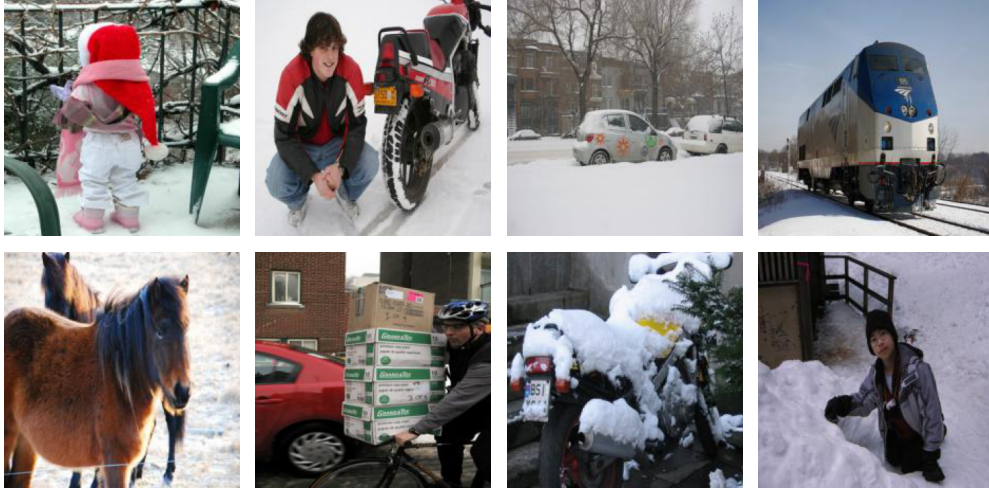


Figure 10: Comparison of ambiguity ranking for **Snow** with Distr. Fit in the top row and U-ACE in the bottom row. Most uncertainty (due to ambiguity) on the left to least uncertainty on the right.

despite employing uncertainty (although in a limited capacity) is likely because simple measurement of uncertainty through MC sampling is not the best method for estimating uncertainty as shown in Table 9.

Dataset	Bayes Regr.	Bayes Regr. with MC	U-ACE
ADE20K	0.39	0.43	0.09
Pascal	0.40	0.45	0.11

Table 10: Significance of prior: quality of explanations severely degrades without the uncertainty-aware prior.

The tables below give a detailed view of the top-10 salient concepts identified using ADE20K for the ResNet-18 scene classification model. The problematic or outlandish concepts are marked in red. We observe that although Bayesian Regr. and Y-CBM are practically the same, the choice of the estimator and sparsity seems to have helped Y-CBM produce (seemingly) higher quality explanations.

Label: **Tree Farm** (ADE20K)

TCAV	palm, horse, pane of glass, helicopter, rubbish, cap, boat, organ, tent, footbridge
Bayes Regr. with MC sampling	net, merchandise, labyrinth, black, big top, ottoman, chest, pigeonhole, tree, sky
Bayes Regr.	oar, forest, pigeonhole, merchandise, sand trap, net, wallpaper, tray, calendar, tree
O-CBM	forest, pot, pottedplant, hedge, trestle, sweater, bush, leaf, foliage, coat
Y-CBM	field, forest, foliage, elevator, gravestone, hedge, bush, vineyard, covered bridge, baptismal font
U-ACE	foliage, forest, grass, field, hedge, covered bridge, tree, leaves, bush, gravestone

Label: **Coast** (ADE20K)

TCAV	shutter, manhole, baby buggy, umbrella, sand, boat, arch, minibike, rubbish, column
Bayes Regr. with MC sampling	wineglass, guitar, headlight, chest, jersey, roundabout, witness stand, magazine, folding door, shaft
Bayes Regr.	lake, headlight, island, hen, dog, chest, jersey, mosque, shaft, windshield
O-CBM	sea, island, lighthouse, cliff, wave, shore, rock, sand, pitted, crystalline
Y-CBM	sea, sand, lake, island, runway, cliff, fog bank, clouds, towel rack, pier
U-ACE	sea, lake, island, pier, cliff, lighthouse, shore, fog bank, water, sand

H.3 Effect of Regularization Strength on Y-CBM and O-CBM

We present the sensitivity analysis for the two strong baselines: Y-CBM and O-CBM in this section.

How are the hyperparams tuned?

Hyperparameter tuning is tricky for concept explanations since they lack a ground-truth or validation set. The reported results for Y-CBM and O-CBM in the main paper used the default value of the regularization strength of the corresponding estimator, which is Lasso³ for Y-CBM and LogisticRegression⁴ for O-CBM. Both the estimators are part of sklearn. We had to reduce the default regularization strength of Y-CBM to $\alpha = 10^{-3}$ so that estimated weights are not all 0. The κ of U-ACE is somewhat arbitrarily set to 0.02 on Broden dataset for sparse explanation with non-zero weight for only 20-30% of the concepts.

Can Y-CBM and O-CBM do much better if we tune the regularization strength?

We present the results of the two baselines for various values of the regularization strength in Table 11. The table shows quality of explanations in the first two rows for the same setup as Table 1 and also shows the measure of drift in explanations like in Table 2. We tried $C=1e-2$, 0.1 , 1 , 10 for O-CBM and $\alpha=1e-4$, $1e-3$, $1e-2$, $1e-1$ for Y-CBM. We dropped $C=1e-2$ and $\alpha=1e-2$, $1e-1$ from the table because then the explanations were overly sparsified to zero.

We observe from the table that U-ACE still is the best method that that yields high-quality explanation while also being less sensitive to shift in the probe-dataset.

I Evaluation using CUB dataset

Wah et al. [2011] released a bird dataset called CUB with 11,788 images and 200 bird species. Moreover, each bird image is annotated with one of 312 binary attributes indicating the presence

³https://scikit-learn.org/stable/modules/generated/sklearn.linear_model.Lasso.html

⁴https://scikit-learn.org/stable/modules/generated/sklearn.linear_model.LogisticRegression.html

Dataset	O-CBM			Y-CBM		U-ACE
Regularization strength \rightarrow	C=0.1	C=1	C=10	$\alpha=10^{-4}$	$\alpha=10^{-3}$	$\kappa=0.02$
ADE20K	0.12	0.20	0.29	0.24	0.14	0.09
Pascal	0.11	0.25	0.35	0.27	0.13	0.11
ADE20K \rightarrow Pascal	0.46	0.26	0.12	0.29	0.34	0.19

Table 11: Results on Broden dataset with varying value of regularization strength for O-CBM and Y-CBM. ADE20K and Pascal rows compare the distance between the explanations computed from the ground-truth exactly like Table 1. The last row compares how much the explanations drifted between the datasets exactly like in Table 2. Lower is better everywhere. Observe that U-ACE has high explanation quality while also being relatively more robust to data shift.

	TCAV	O-CBM	Y-CBM	U-ACE
Top 3	0.38	0.43	0.46	0.43
Top 5	0.39	0.45	0.46	0.44
Top 10	0.37	0.43	0.45	0.42
Top 20	0.36	0.40	0.41	0.39

Table 12: Distance of top-k salient concepts computed using *Oracle* and different estimation methods shown in the first row (lower the better). TCAV does well overall and U-ACE performs the best among methods without access to concept annotations.

or absence of a bird feature. Koh et al. [2020] popularized an improved version of the dataset that retained only 112 clean attribute annotations. We evaluate using the cleaner dataset released by Koh et al. [2020] owing to their popularity in evaluating CBMs. We train a pretrained ResNet-18 model using the training split of CUB dataset. We then compute the explanation (i.e. saliency of concepts) using the test split. Similar to the evaluation of Section 6.1, we quantify the quality of explanations using distance from explanations computed using true concept annotations when using *Oracle*.

	TCAV	O-CBM	Y-CBM	U-ACE
Top 3	0.22	0.17	0.13	0.20
Top 5	0.5	0.33	0.28	0.45
Top 10	1.68	1.18	1.02	1.34
Top 20	5.16	4.185	3.935	4.51

Table 13: Average overlap between top-k salient concepts computed using *Oracle* and different estimation methods shown in the first row (higher the better). TCAV does well overall and U-ACE performs the best among methods without access to concept annotations.